

# Characteristics of Impulse-driven Surface Flashover across Polymers with Different Surface Conditions

Timothy Wong, *Member, IEEE*, Igor Timoshkin, *Senior Member, IEEE*, Scott MacGregor, *Senior Member, IEEE*, Martin Given, *Senior Member, IEEE*

**Abstract**—Power-centric research conducted in the past few decades have identified many influencing factors that affect and contribute to the development of surface flashover. Among them, the surface condition—morphology, roughness, texture—is one such physical characteristic of a gas-solid interface that is believed to be exploitable, relatively inexpensively, as a method to improve surface flashover strength. High voltage pulsed power systems and equipment face similar issues, but there presently exists limited literature focused on impulse-driven flashover and the effects of surface roughness. In this work, the impulse-driven surface flashover strengths of five polymers relevant to pulsed power system design (PVC, Delrin, Ultem, Torlon, Perspex) are reported under two different ( $\sim 20$  nanosecond and  $\sim 100$  microsecond rise-time) impulsive waveforms in atmospheric air. Samples of different surface conditions—“as received” and “machined”—were subjected to flashover tests, complemented with surface profilometry measurements to evaluate the effects of various roughness characteristics on the impulse-driven breakdown strengths and times-to-breakdown. The obtained results indicate a general enhancement of the impulsive flashover strength with increased roughness with a corresponding prolongation of the time-to-breakdown. Rougher “machined” surfaces were therefore found to outperform the smoother “as received” surfaces. A correlation analysis between the measured surface roughness parameters and the breakdown data suggests that the short-wavelength components of the surface profile contributes more towards the enhancement of the flashover strength compared to longer-wavelength “waviness” components. The consistency of this result with the theory of increased streamer path length and streamer inhibition is discussed, as are the potential consequences to insulator surface modification for flashover mitigation.

**Index Terms**—surface flashover, solid-gas interfaces, dielectric phenomena, electrical insulation, pulsed power, electrical breakdown, surface roughness, surface texture

## I. INTRODUCTION

THERE has been significant attention paid to the surface flashover behavior of insulators ever since the realization that gas-solid interfaces presented a greater breakdown risk in composite gas-solid insulated systems. This was based on clear evidence that electrical breakdown strengths across insulator surfaces tended to occur at lower electric field stress than just gas, compromising the hold-off capability of many common insulating systems. The initiation of surface discharges and the development of surface flashover is a multi-faceted issue,

where there are numerous aspects of an electrical system that contributes (to various degrees) towards the overall flashover behavior. The recent review of Li *et al.* [1] provides a comprehensive collation of factors influencing surface flashover behavior in compressed gases, which they broadly organize into the categories: gas parameters, solid parameters, electric field distribution, waveform and charge injection processes, and surface parameters. The present work is primarily concerned with the nature of the energizing waveform (impulse) and with the roughness characteristics of the solid surfaces. As such, a summary of recent works relevant to these aspects is given only; for issues outside of this scope, the reader is referred instead to [1] and references therein for further reading.

In recent efforts to enhance hold-off voltages at gas-solid interfaces, studies have investigated the feasibility and effectiveness of surface modifications on the solid insulator [2]–[5]. Incidentally, this is highly related to studies focused on the effects of surface roughness on surface flashover events [6]–[8]. In general, certain types of rough or modified surface appear to increase the surface flashover strength without compromising on the general mechanical strength of the insulator due to the minimal required changes to the insulator geometry. For example, Zhao *et al.* [7] found increasing flashover voltage for dry silicone rubber (SiR) interfaces with roughness values of  $R_a > 3 \mu\text{m}$ . This was similarly found in Xue *et al.* [6] who attributed the difference to a number of surface changes, including an increase to the surface conductivity with increased roughness. They further find changes to the surface trap distributions that was believed to help suppress the number of available charge carriers participating in a surface discharge. In a series of works by Meyer *et al.* [5], [9]–[11], Marskar and Meyer [12], and in Meyer, Marskar and Mauseth [14]; effects of the purposeful modification of the surface texture, by introducing either square or semicircular surface profiles, was studied experimentally and supported by simulations. Profiles with characteristic dimensions of  $500 \mu\text{m}$  and  $1000 \mu\text{m}$  were studied (far greater than typical roughness features), from which they drew a number of conclusions. They reported an increased hold-off voltage resulting from the impeding of discharge initiation from triple junctions due to the surface profile [5], proposed a streamer re-ignition mechanism that facilitated streamer propagation across textured surfaces [12], and found that narrower profile spacing appeared more effective at inhibiting surface streamer growth.

T. Wong was supported in part by the Engineering and Physical Science Research Council (EPSRC) under grant number EP/T517938/1. For the purpose of open access, the authors have applied a Creative Commons Attribution (CC BY) license to any Author Accepted Manuscript version arising from this submission.

Manuscript received Month XX, 2025; revised Month XX, 2025.

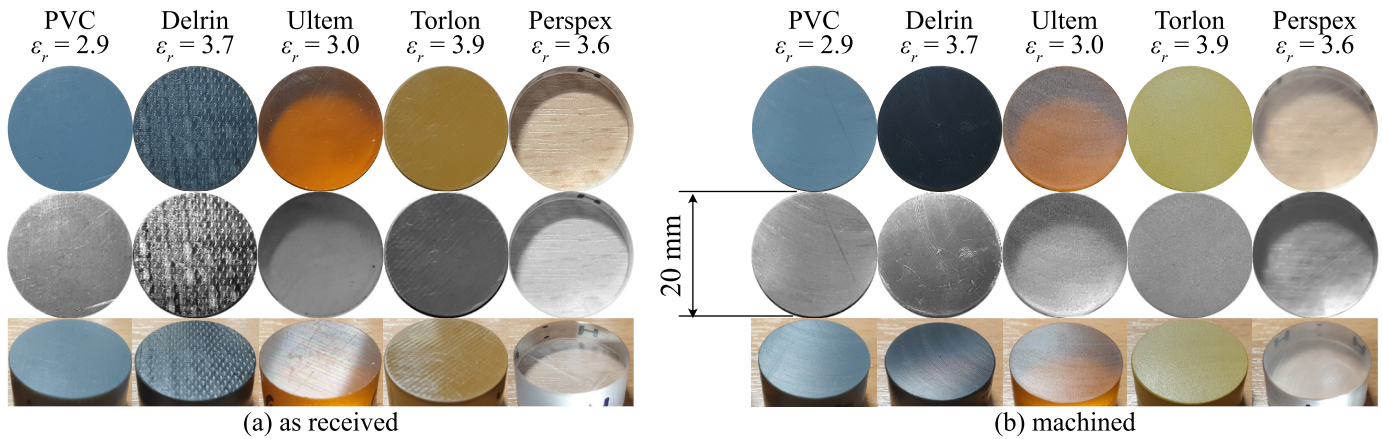


Fig. 1. Photographs and contrast/brightness adjusted photographs of representative sample surfaces used in this work for (a) “as received”, (b) “machined” surfaces with a thin surface layer removed. Brightness and contrast adjusted photographs have been provided as they make the surface features more apparent on some digital displays and in print, for ease of viewing. Note that Perspex has high optical clarity, preventing the surface texture to be easily captured on camera. The wood grain visible in the photograph is that of the table underneath.

Macpherson *et al.* [4] reported similar increases to the hold-off voltage for knurled solid spacers (Ultem, Delrin, and HDPE) under impulse action of around 100 ns rise-time and 700 ns time-to-half for positive energisation. The authors of [4] explain this in terms of the greater path length that required traversal by a positive streamer and the greater voltage required to support its development; an argument similar to those of Meyer *et al.* [12]. Modification of the surface texture on the nanoscale was also attributed to an observed increase in surface flashover strength for ultra-high-molecular-weight polyethylene (UHMWPE) and polymethylmethacrylate (PMMA) samples in Rossi *et al.* [13] for samples treated using the plasma immersion ion implementation (PIII) technique.

Insulator surface modification holds great promise as a low-cost and simple process that could enhance the dielectric performance of gas-solid interfaces within high voltage (HV) power and pulsed power equipment. It is therefore of great importance to gain a deeper understanding of the processes along textured and rough solid surfaces, which ultimately contribute towards the identification of optimal surface profiles that may maximize flashover strength. At the same time, it is equally important to expand the number of materials for which there is reliable empirical characterization data for impulse-driven flashover, as this data is often crucial to support design decisions for practical pulsed power systems development.

In this work, the results of impulsive flashover experiments across five different polymers are presented, which included PVC (polyvinylchloride), Delrin (polyoxymethylene), Ultem (polyetherimide, also known as Duratron U1000), Torlon (polyamide-imide, also known as Duratron T4203), and Perspex (polymethylmethacrylate, or PMMA); under atmospheric pressure laboratory air. These materials were chosen for their commercial availability and common application within pulsed power system components, e.g., see [15]–[17]. Breakdown tests were conducted for two different impulse waveforms and two different surface conditions per material—their surface profiles and roughness parameters quantified by means of profilometry measurements. The experimental arrangements

used to acquire breakdown and roughness data are outlined in Section II, while data processing relating to breakdown statistics and roughness quantification is detailed in Section III. Interpretation and discussion of the attained results follows in Section IV before this work is summarized and concluded in Section V.

## II. EXPERIMENTAL METHODOLOGY AND DATA ACQUISITION

This section describes the experimental arrangements including the nature of the dielectric samples, surface treatment, and the flashover test cell and associated circuit for pulse delivery and flashover tests.

### A. Dielectric Samples

Flat sheets of dielectric material were cut into cylinders of 20 mm diameter and around 10 mm in height—varying between approximately 9 mm to 14 mm in height, since the thickness of each sheet varied. The design of the test cell described in Section II-C compensated for the varying sample heights and ensured identical flashover conditions regardless. One out of the two cross-sectional surfaces of each cylinder was treated using a shoulder mill [18], which removed a thin layer of material from its surface, while the second cross-sectional surface was left untreated. Each sample therefore had two flat surfaces of different surface condition, listed below. Figure 1 encloses photographs showing representative samples of the above-described surface conditions for all materials tested in this work.

- The “as received” surface condition: surface was left untreated *as received* from the supplier/manufacturer, maintaining any existing scratches or surface texture introduced during fabrication or handling.
- The “machined” surface condition: the removal of a thin surface layer also removes any pre-existing scratches or marks that were present on the original surface. These were replaced by faint machining marks due to the rotary action of the shoulder mill during treatment.

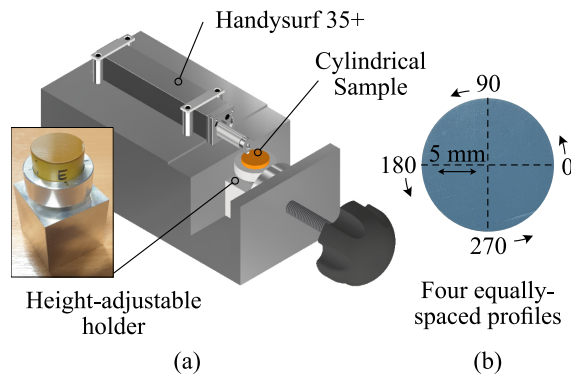


Fig. 2. (a) 3D model of the Handysurf 35+ profilometry system and holder configuration, (b) diagram showing the four measurement locations across which surface profiles were taken for each sample.

Visually, the “as received” surfaces of PVC and Perspex appeared similar, with a mostly smooth appearance and very minor, randomly-oriented, scratches. Ultem and Torlon also appeared similar, but with clear uni-directional parallel lines found across their surfaces, in contrast to PVC and Perspex. The “as received” surfaces of Delrin were distinct from all other materials, with surfaces covered with small indentations. These indentations were uniformly spaced, and evidently, intentionally placed. However, their size, shape, and density varied across different samples of Delrin. Some samples had indentations that appeared closer to a diamond-like shape, while other were circular in nature, and were found to vary in both depth and size. The exact source of these surface features is not clear, but undoubtedly results from some process related to the method of manufacture.

The “machined” surfaces were visually similar across all materials, with faint (curved) machining marks due to the rotary action of the tool. It is further remarked that the Torlon samples used here were comprised of three layers, where the thinner dark-brown outer layers have resulted due to curing processes during production [19]. The machining process for the “machined” condition therefore strips away one of these cured layers, exposing the material underneath. This was taken as an opportunity to evaluate whether the inner layer would have any tangible difference to the flashover properties of Torlon.

### B. Surface Profilometry System

Prior to breakdown tests, measurements of the surface profiles of each individual sample was conducted using the Handysurf 35+ manual profilometer [20]. The methodology is similar to that of a related study by the authors [21] differing only in the geometry of the samples in this case, for which an additional holder was fabricated to facilitate four surface profiles to be taken per sample, as illustrated in Figure 2. The reader is referred to the details of [20], [21] for additional information regarding the instrument and details of its usage. These surface profiles were taken at equally-spaced intervals along the radial direction, providing a reasonable measure of the gross surface morphology. The treatment of the obtained surface roughness data is described in Section III-A.

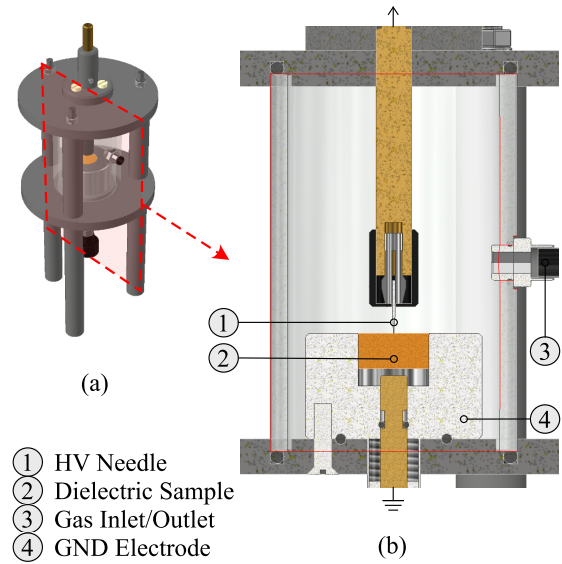


Fig. 3. 3D model of the custom test cell used for impulsive flashover tests. (a) Perspective view of the full test cell, (b) sectional view cut through the center plane, with labels provided for key components.

### C. Breakdown Test Cell and Circuit

Surface flashover tests were conducted using a custom test-cell incorporating a concentric and rotationally-symmetric design, a 3D model of which has been provided as Figure 3. The cylindrical dielectric samples were inset into the ground electrode such that the surface under test would sit flush with its top surface, resting atop a height-adjustable threaded rod. The ground connection was designed to allow for height adjustment to compensate for the different thicknesses of the various dielectric samples. A small piece of fabric was additionally placed between the rod and the bottom surface of the sample, preventing the possibility of contact damage of the surface from the rod when samples were adjusted or removed between experiments.

Breakdown was induced across the sample surfaces by application of HV impulses to the needle electrode (“soft-tone” gramophone needles) of approximately  $80 \mu\text{m}$  tip radius, held directly above the center of the sample. Effort was made to ensure that the needle tip would be as centered as possible to reduce the chance of preferential breakdown paths due to one side of the needle being closer to the ground electrode edge. The resulting triple junction formed between the needle, dielectric, and air ensured that discharges would initiate from the needle tip and propagate across the sample surface with greatest probability. Five needles closest to the target  $80 \mu\text{m}$  tip radius were selected from a pack, done via the inspection of each needle under a microscope and a measurement of the tip radius. The final five needles had a mean tip radius of  $80.38 \pm 5.59 \mu\text{m}$ , and which were replaced after the completion of tests on 16 samples ( $16 \times 20$  HV shots per sample = 320 shots per needle—see Section II-D). This was informed by needle degradation tests performed using a separate test needle, for which a dummy sample was subjected to  $>600$  shots and was re-inspected for tip deformation or damage. Due to the low

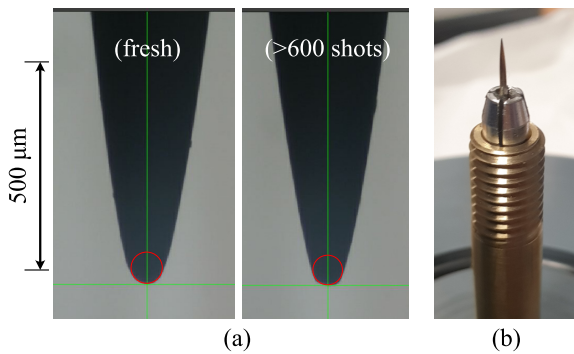


Fig. 4. (a) Microscope images of magnified gramophone needles used as the HV electrode in this work; comparing the same needle before and after over 600 HV shots with no degradation, (b) photograph of the needle electrode held within the brass HV connection, with the securing plastic cover removed.

pulse energy of the systems used in this work, the needle geometry was found to be unchanged with no visible damage, providing confidence in the consistency of each test. Figure 4 compares two microscope images of this test needle before and after degradation testing.

The test circuit used in this work is shown in Figure 5, where the generic *pulse generator* component represents one of two pulse generation systems: (i) a Samtech TG-01 generator capable of  $\sim 100 \mu\text{s}$  rise-time impulses at  $\sim 35 \text{ kV}$  peak voltage; or (ii) a stacked Blumlein generator following the topology of [22], outputting  $\sim 20 \text{ ns}$  rise-time impulses of around  $60 \text{ kV}$  peak voltage. The latter was charged through a Glassman HV power supply through a  $1 \text{ M}\Omega$  resistor at  $15 \text{ kV}$  charging voltage, and was operated via the self-breakdown of an air-filled spark gap. It must be noted that under the configuration described here, consistent breakdown on the rising edge could only be achieved using the Samtech TG-01 system, while breakdown occurred on the falling for all Blumlein flashover events. Consequently, both breakdown voltage and time-to-breakdown could be recorded for all Samtech TG-01 tests, while only breakdown time could be inferred based on the breakdown current waveform for all Blumlein tests. The methods used to extract these quantities from the raw oscillograms are described within Section III-B.

In the case of the lower peak voltage Samtech generator, voltage monitoring was configured using a Tektronix P6015A high voltage probe, while the faster-rising Blumlein system was equipped with a copper sulphate voltage divider connected to a Northstar PVM-5 high voltage probe. In the latter case, current monitoring was also used as a means to identify the times-to-breakdown through a Pearson 6585 current transformer. All waveforms were captured on a Tektronix TDS3054C digital oscilloscope.

#### D. Experimental Procedure

Sample preparation involved first taking surface roughness measurements of the sample surfaces, following Section II-B. Each surface was then cleaned using a 70% ethanol-water solution using low-lint paper and allowed to dry. Samples were then inserted into the test cell, height adjusted, and needle electrode lowered to rest on the sample surface. The test cell

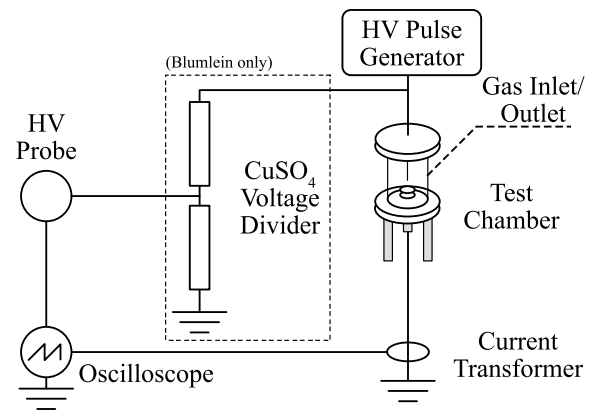


Fig. 5. Circuit diagram of the experimental test circuit used in this work. The HV pulse generator was either a custom-built stacked Blumlein triggered using a self-breaking spark gap, or a Samtech TG-01 trigger generator; details of diagnostics provided in main text.

was sealed and flushed with fresh laboratory air after each shot, which were similarly separated by 1 min 30 s as in [21].

Two independent surfaces of the same material and surface condition were subjected to 20 HV shots each, to ensure consistency for the same material-condition pairs. However, the first 20 and second 20 shots are treated as separate datasets during data analysis since their roughness conditions may be similar but not identical. Following Section II-C, the needle was replaced every 320 shots (16 samples).

### III. DATA PROCESSING

In total, raw profilometry data included  $5 \text{ materials} \times 4 \text{ measurement locations} \times 2 \text{ polarities} \times 2 \text{ rate-of-voltage-rise } (dU/dt) \times 2 \text{ surface conditions} \times 2 \text{ independent surfaces per condition} = 320 \text{ surface height profiles}$ . Raw breakdown data included  $5 \text{ materials} \times 2 \text{ polarities} \times 20 \text{ shots per surface} \times 2 \text{ surface conditions} \times 2 \text{ } dU/dt \times 2 \text{ independent surfaces per surface condition} = 1600 \text{ sets of oscillograms}$  incorporating voltage and/or current measurements. The data processing methods used to extract the desired information from the gathered raw data is described in this section.

#### A. Surface Roughness Characterization

As in [21], the *motif* method was used to calculate characteristic roughness and waviness parameters for each surface following the ISO-12085 standard [23]. Namely, the parameters of interest include  $R$ ,  $W$ ,  $AR$ , and  $AW$  which are hereby referred to generally as the *motif parameters* as described in Table I. The former,  $R$  and  $W$ , give a general indication of the heights of short-wavelength components of the surface; while the latter,  $AR$  and  $AW$ , correspond broadly to the longer-wavelength undulations of the surface profile. In addition, the *compound surface parameters*,  $\eta$ ,  $\sigma$ ,  $\beta$  and  $a$ , were also computed from the motif parameters as a further means of surface texture quantification, based on the method of [24], [25]. All meanings of the above parameters, including units, have been included in Table I. Both the motif and compound surface parameters were independently calculated for all four

TABLE I  
DESCRIPTION AND UNITS FOR THE MOTIF AND COMPOUND SURFACE  
PARAMETERS USED WITHIN THE PRESENT ANALYSIS.

Param.	Description	Typ. Units
$R$	Mean height of roughness motif profile	$\mu\text{m}$
$W$	Mean height of waviness motif profile	$\mu\text{m}$
$AR$	Mean width of roughness motif profile	mm
$AW$	Mean width of waviness motif profile	mm
$\eta$	Surface asperity density	$\text{mm}^{-1}$
$\sigma$	Standard deviation of asperity heights	$\mu\text{m}$
$\beta$	Mean surface asperity radius	$\mu\text{m}$
$a$	Mean asperity aspect ratio	1

measured profiles per surface, before the arithmetic mean was computed for each unique surface.

### B. Statistical Treatment of Flashover Data

The flashover characteristics of interest included the breakdown voltage,  $V_{br}$ , and the time-to-breakdown,  $t_{br}$ . For the slower-rising Samtech TG-01, the same method as in [21] was employed. In brief, this firstly involved the low-pass filtering of raw voltage waveforms to reject noise and identify an unambiguous peak breakdown voltage; while the time-to-breakdown was taken between the first zero-crossing nearest the rising edge to the time of the waveform peak.

As mentioned within Section II-C, breakdown on the rising edge could not be attained using the faster-rising Blumlein generator, likely due to the higher overstressed breakdown voltage for the substantially greater value of  $dU/dt$  compared to the TG-01. As such, this work reports only times-to-breakdown for the Blumlein case, which required an alternative method of determination. Using both current and voltage waveforms, the Blumlein times-to-breakdown were taken as the time between the first zero-crossing of the voltage nearest the rising edge to the beginning of the rise in breakdown current. All identified values were manually inspected to ensure that the correct points were identified.

The 20 datapoints per surface were fit to 2-parameter Weibull distributions using Maximum Likelihood Estimation (MLE) informed by Kolmogorov-Smirnov and Lilliefors tests at 95% confidence. In this case, the characteristic breakdown voltage is taken to be the 63.2% probability failure voltage ( $V_{63.2} = V_{br}$ ); while the statistical time-to-breakdown is assumed to be given by the corresponding  $t_{63.2} = t_{br}$ , under the assumption that the formative breakdown time is negligible in comparison.

## IV. RESULTS AND DISCUSSION

This section presents and discusses the obtained results in three parts. Section IV-A conducts a comparison of the pre-breakdown surface conditions of the “as received” and “machined” surfaces over all samples. Section IV-B then reports on the measured breakdown voltages and times for all conducted flashover experiments, before Section IV-C presents the results of a correlation analysis between the experimentally-determined surface roughness and flashover parameters.

### A. Pre-breakdown Surface Comparison

Figure 6 includes histograms of the computed motif and compound surface parameters across all samples, which have been plotted to facilitate comparison between the “as received” and “machined” surface conditions. By comparing across all materials, any change in the distribution represents, in general, the effects of the machining action on the gross surface morphology. Each pair of distributions of the same parameter were additionally evaluated using 2-parameter Kolmogorov-Smirnov tests to determine the likelihood that the two sets of data are likely to belong to the same distribution. Tests at 95% confidence were conducted, with the corresponding significance ( $p_s$ -values) indicated in Figure 6. A value of  $p_s < 0.05$  was considered statistically significant. These tests were conducted using the MATLAB `kstest2()` function with the gathered experimental data used as input.

Statistically significant shifts in the distributions for all motif and surface parameters was found except for  $AW$ , a parameter associated with the width of long-wavelength surface features. Qualitatively, clear changes in the distributions for parameters relating to short-wavelength roughness parameters (e.g.,  $R$ ,  $W$ ,  $\sigma$ ,  $\beta$ , and  $a$ ) was observed, supported by the substantially smaller significance values. Overall, the greatest change after machining was found for parameters which relate to the short-wavelength roughness features, while the longer-wavelength (waviness) variations of the profile were modified to a lesser extent. Similarly, the motif profile *heights* were modified to a greater extent compared to the profile *widths*.

### B. Breakdown Voltage and Time

This section concerns itself with the presentation and interpretation of the impulsive flashover results. Breakdown voltages and times-to-breakdown for tests conducted using the Samtech TG-01 generator are first discussed as presented in Figure 7(a)–(b). Examples of typical open-circuit and breakdown waveforms for both generators have been included in Appendix A. It is clear, from Figure 7(a)–(b), that under the present configuration, negative-polarity breakdown voltages were several kilovolts lower than positive breakdown voltages for all tests. Given that asymmetric electrodes were employed in this study, it is unsurprising to find clear polarity effects. In this case, the difference can be explained using streamer theory and by considering that the utilized electrode geometry incorporates two triple junctions.

Consider that the first is located at the tip of the needle electrode, where it sits in contact with the sample; and the second, where the dielectric sample meets the inner edge of the ground electrode. Figure 8(a) shows the simulated electric field distribution in the test cell, numerically computed using QuickField Professional [26] at a voltage of 30 kV. Labeled on the figure is a contour along sample and ground electrode surface, along which the electric field strength is plotted in Figure 8(b). It is shown that the electric field can exceed the critical field of air of around 3 kV/mm when the voltage pulse reaches its maximum (and any irregularities present on the practical electrodes may see the true value be even greater). Thus, positive and negative streamers have the potential to

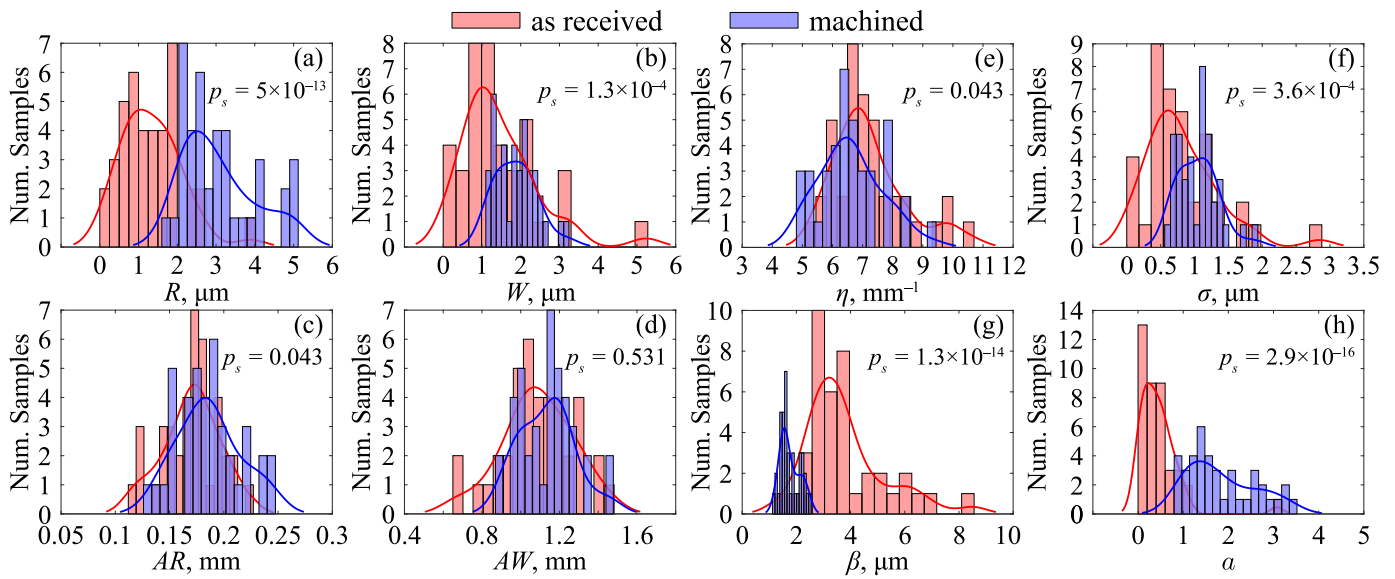


Fig. 6. Histograms of the averaged motif parameters (a)  $R$ , (b)  $W$ , (c)  $AR$ , (d)  $AW$ , and compound surface parameters, (e)  $\eta$ , (f)  $\sigma$ , (g)  $\beta$ , and (h)  $a$  based on the combined data for all samples of all materials split into “as received” and “machined” surfaces. Solid lines are kernel density estimates (KDE) fitted to the empirical distributions, for visual guidance only. Indicated  $p$ -values were computed from 2-parameter Kolmogorov-Smirnov tests between “as received” and “machined” distributions, where  $p < 0.05$  is considered a statistically significant difference due to machining at 95% confidence. Full dataset of averaged parameters for each material can be found within Figures S1 and S2 of the supplementary material associated with this paper.

initiate from both points during the pre-breakdown phase and propagate towards each other. However, the asymmetry and vastly different geometries of the two electrodes imparts a far stronger field at the needle triple junction compared to the junction of the ground electrode. As is established in the literature (e.g., [27] and references therein), positive streamers tend to initiate at lower field magnitudes, but negative streamers typically exhibit greater acceleration and attain higher propagation velocities than their positive counterparts once incepted. It follows that under positive impulse action, a positive streamer may incept far earlier at the needle and begin to propagate along the surface, while the negative streamer remains within its initiating phase (or has not started to propagate) near the ground electrode triple junction. To bridge the electrode gap, the positive streamer therefore traverses a greater proportion of the inter-electrode gap before combining with the negative streamer. This leads to the behaviour of the positive streamer having a greater impact on the breakdown behaviour of the surface. The lower value of  $dU/dt$  of the Samtech TG-01 generator may additionally lead to the suppression of negative streamer formation altogether due to the action of outward electronic diffusion during the rising slope. In this case, the positive streamer would be required to traverse the entire 1 cm gap distance before the electrodes become bridged.

In contrast, under negative-polarity impulses, negative streamers are believed to reach the propagation phase at almost the same time (or earlier) as a positive streamer originating from the ground triple junction. The greater electric field strength at the needle compensates for the typical initiation delay observed for negative streamers. As such, a pair of positive and negative streamers may simultaneously develop across the surface, each traversing some proportion of the inter-electrode gap distance, leading to an overall shorter

breakdown time and therefore a lower breakdown voltage. Simulations or experimental imaging of surface streamers may be used in future to test this idea further, but is deemed outside the scope of the present work.

For the faster-rising impulses of the Blumlein, Figure 7(c)–(d) encloses the extracted times-to-breakdown. Under positive-polarity Blumlein impulses, flashover tended to occur earlier and closer to the voltage peak, while negative impulses consistently exhibited breakdown at a comparatively late time, on the falling edge. This explains the significant time difference between positive and negative times-to-breakdown seen in Figure 7(c)–(d). This difference additionally suggests that the negative impulse breakdown voltage would be higher than the positive case, if both were to be achieved on the rising slope, contrasting the case of the TG-01. However, this effect may also be a result of breakdown on the falling edge and may be related to a minimum field required to sustain streamer propagation. A stronger electric field is typically necessary to both initiate and to sustain negative streamer propagation due to their more diffuse nature. As the voltage begins to decrease from the peak, it may be the case that the decrease in the field acts to slow the development of negative streamers to greater effect than on positive streamers; the latter of which have more compact wavefronts and can generally be sustained at lower field magnitudes. This may provide an additional factor contributing to the delay of negative polarity breakdown when occurring on the falling edge. Overall, no significant differences were found between different materials.

Notable tendencies can additionally be observed when comparing between “as received” and “machined” surfaces. For the TG-01 tests, “as received” surface tended to exhibit flashover at a generally lower voltage than “machined” surfaces, but exclusively for negative impulses. For positive-polarity tests,

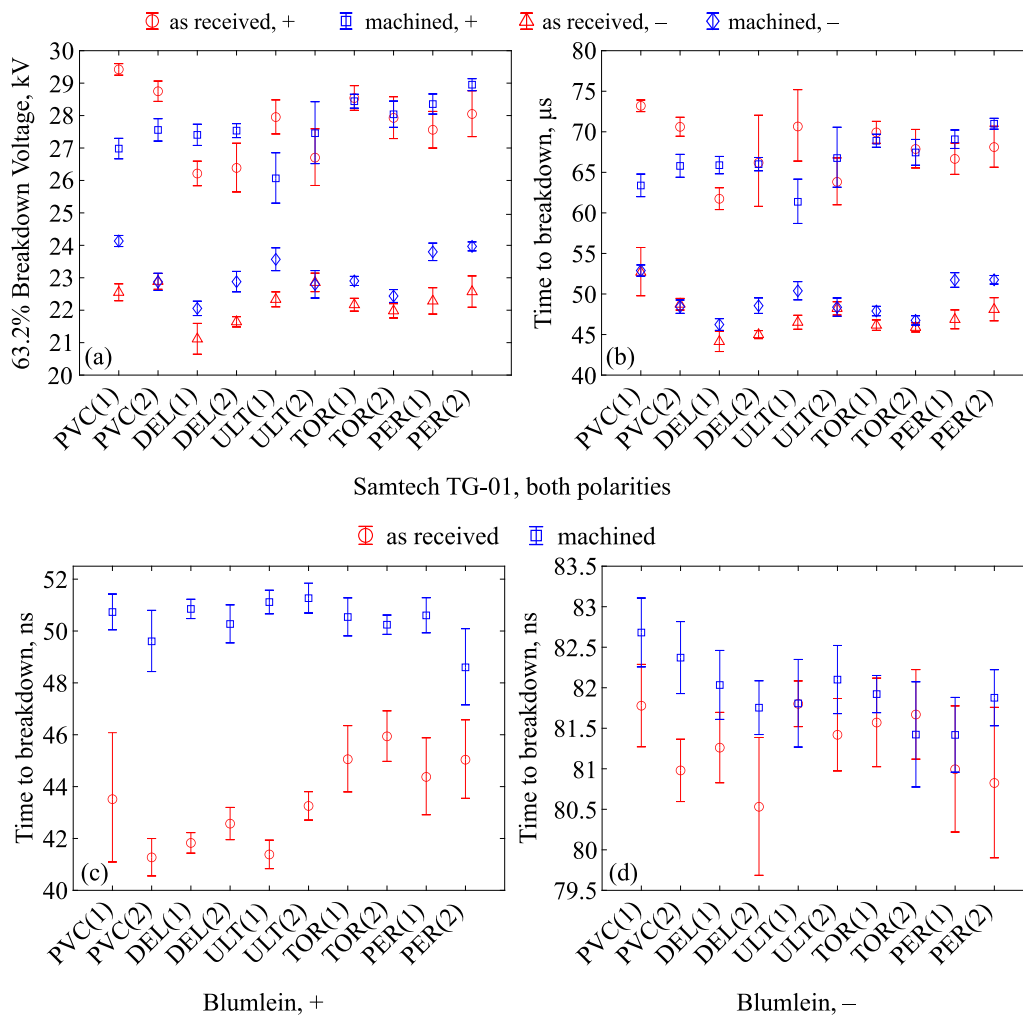


Fig. 7. 63.2% (a) breakdown voltage and (b) time-to-breakdown for surface flashover events using the Samtech TG-01 generator for both surface conditions and polarities. 63.2% time-to-breakdown for Blumlein flashover events for (c) positive polarity and (d) negative polarity impulses. Error bars indicate the 95% confidence intervals.

no such distinction was found. It is possible that the more diffuse nature of negative streamer fronts are more prone to interruption by changes in surface morphology, and may be more difficult to reignite once interrupted compared to their positive counterparts. However, this does not align with the tendencies observed for the Blumlein tests, suggesting other mechanisms that remain unaccounted for. In the Blumlein case, this tendency emerges in the time-to-breakdown data for both polarities: the “as received” surfaces typically experienced flashover earlier than “machined” surfaces, with positive Blumlein tests breaking, on average, by around 9 ns earlier compared to a difference of 1 ns to 3 ns for the negative case. The differences in surface conditions are believed to be responsible for the tendencies of the TG-01 negative and Blumlein results of both polarities, as explained in the following.

In consideration of the profilometry results of Section IV-A, it is believed that the increase in surface profile heights ( $R$  and  $W$ ) may act to impede surface discharges by increasing the effective path length. Pre-breakdown streamers tend to adhere to surfaces as shown in [28], [29], thus, any additional degree

of surface corrugation or irregularity tends to increase the total length a streamer must travel to bridge the electrode gap, believed to prolong the time-to-breakdown [4], [5], [12].

Additional analysis may be based on mechanisms described in the series of combined works conducted by Meyer *et al.* [5], [14], [30] and Marskar [12], who investigated streamer propagation along profiled surfaces of various geometry. The corrugated surfaces of various profiles used in [12], [14] had surface features which were far more uniform and of significantly larger characteristic scale (minimum 500  $\mu\text{m}$  between corrugations) than typical surface asperities found on the present samples. However, reported effects of the impeding and suppression of surface streamers are believed to be highly relevant to the interpretation of the present results. The authors of [12] concluded that smaller spacing between profile features reduced the streamer propagation distance over the same time, which aligned with the increased breakdown strengths observed experimentally in [5] and in the tests conducted in this work. Simulations in [12] also indicated that the main driving mechanism could be attributed to the increase in discharge path length, but also the inability for

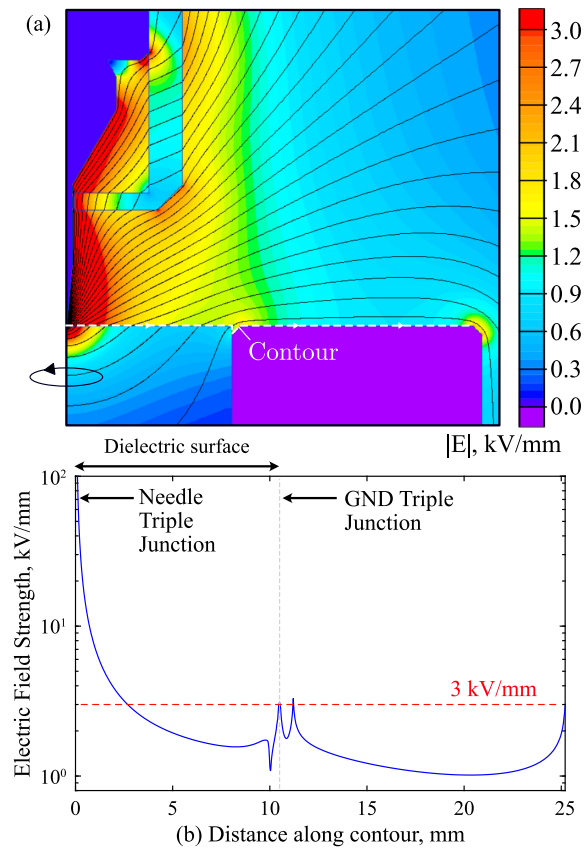


Fig. 8. (a) QuickField simulated electric field distribution inside the test cell at a peak applied voltage of 30 kV magnified to the dielectric surface ( $\epsilon_r = 3$ ), (b) electric field magnitude across the dielectric surface and ground electrode, corresponding to the contour of (a). Red dashed line shows 3 kV/mm as a reference value for the critical field strength of atmospheric air.

streamer re-ignition and subsequent re-connection between adjacent surface features. Their theory is largely consistent with the majority of the results found here, considering that a rough surface is morphologically similar to a corrugated surface, with the difference that the distribution of surface features is non-uniform, and the features themselves are on the scale of several micrometers instead.

However, the current theories do not consider the effects of impulse rate-of-rise and cannot explain several discrepancies in the present data. Namely, why positive flashover across the PVC(1), PVC(2) and ULT(1) surfaces for the TG-01 tests [Figure 7(a)] were found to stray from this behavior, with “as received” surfaces outperforming those that were machined. These may suggest behavior specific to longer-rising positive impulses, of PVC, or may simply be the effect of the limited number of samples. In any case, it would be of great interest to substantially expand the range of surface roughness conditions and  $dU/dt$  values under test to supplement the present results, which has been planned for a future study to clarify these observations.

### C. Correlation Analysis of Flashover and Surface Characteristics

To better understand the effects of individual surface characteristics on the measured flashover voltages and times, this

TABLE II  
MATRIX OF CALCULATED SPEARMAN'S CORRELATION COEFFICIENTS AND SIGNIFICANCE VALUES FOR ALL SURFACE FLASHOVER/ROUGHNESS DATASETS.

TG-01 +	$R$	$W$	$AR$	$AW$
$\rho_c$	-0.149	-0.135	-0.183	-0.123
$p_s$	0.530	0.568	0.437	0.603
Blumlein +	$R$	$W$	$AR$	$AW$
$\rho_c$	<b>0.293</b>	0.227	0.185	<b>0.299</b>
$p_s$	<b>0.209</b>	0.334	0.433	<b>0.199</b>
TG-01 -	$R$	$W$	$AR$	$AW$
$\rho_c$	<b>0.504</b>	-0.038	0.071	<b>-0.392</b>
$p_s$	<b>0.025</b>	0.876	0.767	<b>0.088</b>
Blumlein -	$R$	$W$	$AR$	$AW$
$\rho_c$	<b>0.268</b>	0.212	-0.238	-0.057
$p_s$	<b>0.253</b>	0.368	0.312	0.811
TG-01 +	$\eta$	$\sigma$	$\beta$	$a$
$\rho_c$	0.183	-0.132	-0.038	-0.021
$p_s$	0.437	0.577	0.876	0.932
Blumlein +	$\eta$	$\sigma$	$\beta$	$a$
$\rho_c$	-0.185	0.156	-0.205	<b>0.262</b>
$p_s$	0.433	0.509	0.385	<b>0.264</b>
TG-01 -	$\eta$	$\sigma$	$\beta$	$a$
$\rho_c$	-0.071	-0.039	<b>-0.501</b>	<b>0.510</b>
$p_s$	0.767	0.871	<b>0.022</b>	<b>0.023</b>
Blumlein -	$\eta$	$\sigma$	$\beta$	$a$
$\rho_c$	0.238	0.253	<b>-0.561</b>	<b>0.501</b>
$p_s$	0.312	0.281	<b>0.011</b>	<b>0.026</b>

section combines the breakdown data of Section IV-B and the surface data of Section IV-A in a correlation analysis and discusses the implications of the results. The method used here was as follows. For each dataset pertaining to an independent combination of  $dU/dt$  and polarity, the extracted  $V_{br}$  or  $t_{br}$  were correlated against the set of motif parameters  $R$ ,  $W$ ,  $AR$ ,  $AW$ , and the set of compound surface parameters,  $\eta$ ,  $\sigma$ ,  $\beta$ , and  $a$ . As a quantitative measure of correlation, Spearman's correlation coefficient,  $\rho_c$ , was calculated between the breakdown voltages/times and each surface parameter according to

$$\rho_c = \frac{\text{cov}[\mathcal{R}(x), \mathcal{R}(y)]}{\bar{\sigma}_{\mathcal{R}(x)} \bar{\sigma}_{\mathcal{R}(y)}} \quad (1)$$

where  $\text{cov}(\cdot, \cdot)$  is the covariance between the function arguments, the function  $\mathcal{R}(\cdot)$  represents the *rank* of the variable within the data vector (in this case,  $x$  and  $y$  represent a pair of voltage/surface or time/surface parameters), and  $\bar{\sigma}_{\mathcal{R}(\cdot)}$  is the standard deviation of the extracted variable ranks. Spearman's correlation coefficient can be considered a measure of whether variables  $x$  and  $y$  are correlated by a *monotonic* function which is not necessarily linear (unlike Pearson's correlation coefficient, which measures linear correlations only). The reader is reminded that  $\rho_c$  has a range  $[-1, +1]$ , where a value close to  $-1$  indicates a strong monotonically decreasing correlation, while a value close to  $+1$  suggests a strong monotonically increasing correlation. The calculated values of  $\rho_c$  for each dataset has been included in Table II alongside the corresponding significance values,  $p_s$ , as a measure of the confidence that the calculated correlation coefficient is indeed non-zero.

It is remarked that considerably larger datasets (beyond the 20 points per dataset gathered here) would substantially improve the power of a correlation analysis. Statistical sig-

nificance at a standard 95% confidence is unlikely to be attained for smaller sample sizes of this nature. However, several tendencies observed from the overall comparison of the calculated  $\rho_c$  and  $p_s$  value pairs nonetheless warrants discussion. From Table II, surface parameters that appeared most correlated (and with greatest confidence that a correlation does exist) to the surface flashover characteristics are the mean asperity radius,  $\beta$ ; and the asperity aspect ratio,  $a$  (highlighted in green and in **bold** in Table II). In fact, statistical significance at >95% confidence was found for  $\beta$  and  $a$  parameters for all negative flashover tests, providing reasonable grounds to suggest that there are moderate ( $|\rho_c| \approx 0.5$ ) correlations between these features to the impulse breakdown voltage and time. This was, however, less clear for all positive tests regardless of  $dU/dt$ , which may additionally suggest that these sharper surface features (as suggested by greater values of  $a$ ) have a greater inhibition effect on the more diffuse, negative-polarity, streamers.

The next most-significant correlations based on Table II are highlighted in blue and in *italics*. These correspond to correlations with moderate values of  $|\rho_c| \gtrsim 0.3$  at around 75% confidence ( $p_s \lesssim 0.25$ ). Those that fell into this category included the roughness motif heights,  $R$ , once again suggesting that the increase in height of the short-wavelength components of the surface profile has a strong influence on evolution of surface flashover. Two other correlation values that fit into this category were both related to the waviness motif width,  $AW$ . However, the nature of these correlations are of opposite sign between the positive Blumlein dataset and the negative TG-01 dataset—which seemingly suggests an increase to the flashover voltage (time) for the former case but a decrease to the latter. Considering also the low confidence of the other two correlation coefficients concerning the  $AW$  parameter, these two statistics are perhaps best interpreted with some caution, and would benefit from an expanded study with a larger data sample. Additionally, despite the statistically significant change in the distribution of the waviness height parameter,  $W$ , after machining [as in Figure 6(b)], there is little to suggest that this correlated to a change in the flashover voltage or time. The correlation coefficients concerning  $W$  were found to be generally higher for Blumlein tests, but the significance values lend little confidence to this observation. Since  $W$  measured the heights of the waviness motif, it may suggest that the long-wavelength features of the surface profile are of lesser impact to the overall evolution of surface flashover. For the positive TG-01 dataset, none of the calculated correlation coefficients satisfied even the loosened significance criteria, likely due to the effects of the PVC(1), PVC(2) and ULT(1) results as briefly discussed in Section IV-B.

From the present results, it is believed that there exist some physical basis for the observed correlations. The parameters  $R$ ,  $\beta$ , and  $a$  are broadly indicative of the degree of *protrusion* away from the surface median of short-wavelength surface asperities. From the perspective of streamer inhibition, it seems reasonable that taller asperities (and sharper, higher aspect-ratio asperities) would present as more difficult obstacles for a propagating streamer, and lead to a more substantial increase in the effective streamer path length. It is hypothesized that

for micro-profile features (including surface roughness) on a similar dimensional scale to the characteristic features of streamers (e.g., charge sheaths, streamer head radii) may most strongly facilitate streamer inhibition during the pre-breakdown stages. Larger changes to surface undulations (represented here by the waviness and long-wavelength surface parameters) across distances far greater than streamer characteristic scales, may ultimately provide little contribution to an increase of the effective path length, limiting their effectiveness for the suppression of streamer development. From a practical point of view, surfaces used “as received” from the supplier were generally smoother than those that were “machined” both in terms of roughness and waviness. Both were found modified by the action of machining, but it appears that the changes to the short-wavelength surface features contributed more strongly to a measurable increase in the impulse-driven flashover voltage and prolonged flashover time found for the majority of cases. There did not appear any observable differences between materials, at least for the selection of polymers used in this work and in the chosen experimental configuration.

To summarise, the Spearman correlation coefficients calculated for the present data indicate that broadly, asperity radii and aspect ratio appear to be stronger determinants of breakdown strengths for surface flashover, with the other short-wavelength roughness parameters ranking second as possible factors. Other longer-wavelength roughness parameters correlate far less strongly with breakdown strengths. Additionally, it was discussed how these may relate to surface streamer characteristics in terms of the potential ease for the streamers to be interrupted due to surface features of different length scales.

## V. CONCLUSIONS

The present work has presented the results gathered from surface flashover experiments under HV impulse action in atmospheric (laboratory) air. The present work focused on the comparison between fresh, “as received”, surfaces and treated, “machined”, surfaces that were of different surface condition. The results from combined profilometry and impulsive flashover tests were reported for five polymers relevant to pulsed power systems: PVC, Delrin, Ultem, Torlon, and Perspex; and under two different impulse conditions ( $\sim 100 \mu\text{s}$  and  $\sim 20 \text{ ns}$  rise-time) of positive and negative polarities. The obtained results have deepened the understanding of the effects of surface condition on the impulse-driven flashover characteristics of polymeric insulation, contributing towards the development and optimization of next-generation composite insulating systems for pulsed power equipment. A summary of the key points include:

- For the polymers used in this work, surface profilometry and motif characterization indicated a statistically significant increase to the heights of short- and long-wavelength surface features after machining action. Long-wavelength undulations were affected to a lesser extent, and lesser change was also found for motif profile widths.

- The machining method used here increased the surface asperity heights and asperity radii of the “as received” material samples, producing surfaces with generally greater overall *roughness* but less, but still significant, change to *waviness*.
- There was no indication of substantial differences in flashover strength (or flashover time) between materials.
- There did not appear to be substantial differences in flashover behaviour between different  $dU/dt$  aside from increases to the breakdown strength as is expected for faster-rising impulsive gas breakdown.
- Breakdown results suggest that “machined” surfaces generally experienced flashover at higher voltages than “as received” surfaces.
- A correlation analysis using Spearman’s correlation coefficient suggests that short-wavelength surface features have a stronger influence on the surface flashover voltage than long-wavelength surface variations.
- Overall, rougher (machined) surfaces therefore enhanced surface flashover strengths, in agreement with previous results and with the theory of increased path length and suppression of surface streamer development.
- Wavier surfaces alone appear to have lesser effect since the effective path length is not substantially increased, and do not pose the same degree of irregularity for effective streamer interruption or mitigation.

The empirical data reported from this study may additionally provide critical design knowledge for existing and future surface-modified solid insulators. This acts as additional performance data important for the selection of appropriate materials for pulsed power systems development that employ similar geometries and waveforms used in this work. The results may further aid in the development and optimization of specific surface profiles to be applied to solid dielectric spacers in terms of shape, size, and distribution for the greatest enhancement of surface flashover voltage. For current power and pulsed power systems equipped with insulation systems that cannot be easily redesigned, surface texture modification may provide a potential route for flashover improvement with minimal modification to system topology. Future novel insulating structures may additionally benefit from this work as it may provide guidance on whether surface texture should be factored into system development and during insulation coordination. There inevitably exists significant scope for further work, owing to the many facets of impulsive surface flashover that remain poorly understood. Some recommendations include

- Systematic discharge modeling studies, conducted using complex surfaces designed to emulate practical rough surfaces, would be highly beneficial to further understand the effects of surface condition and irregularity on surface streamer development.
- Given past and present results on the posited influence of surface texture on streamer inhibition across interfaces, can optimal profiles and/or optimal features of profiles be identified to maximize the enhancement of flashover strength (relating to spacing, distribution, and shape).

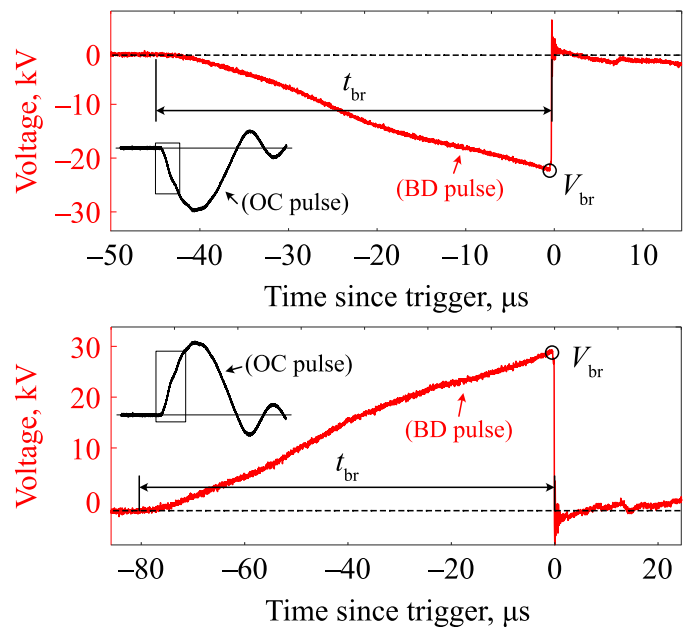


Fig. 9. Typical Open-circuit (OC) and Breakdown (BD) voltage waveforms for (top) negative, (bottom) positive voltage energisation using the Samtech TG-01 pulse generator. Indicated are points used to compute the time-to-breakdown,  $t_{br}$ , and breakdown voltage,  $V_{br}$  as described in the main text. OC waveforms have been inset to show the full pulse, which followed a half sine wave profile and which peaked at around  $100 \mu s$ .

- Further expansion of this study to include a wider range of materials, energisation regimes, electrode geometries, and surface conditions.
- Expansion of the types of surface condition to reflect other, commonly used, industrial surface treatment methods. Understanding the changes these may have on the surface condition depending on the method used, and any corresponding effects on the surface flashover behavior.

#### ACKNOWLEDGMENTS

The authors gratefully acknowledge Andrew Carlin, Sean Doak, Scott Gubbins, and Louis Cooper for their aid in test-cell fabrication and sample preparation.

#### APPENDIX A

##### OPEN-CIRCUIT AND BREAKDOWN WAVEFORMS

Figure 9 and 10 show typical examples of open-circuit and breakdown voltage waveforms, for the two different generators used in this work—the Samtech TG-01 and the Blumlein pulse forming line, respectively.

#### REFERENCES

- [1] Z. Li, J. Liu, Y. Ohki, G. Chen, H. Gao, and S. Li, “Surface flashover in 50 years: Theoretical models and competing mechanisms,” *High Volt.*, vol. 8, no. 5, pp. 853–877, 2023.
- [2] C. Li, J. he, and J. Hu, “Surface morphology and electrical characteristics of direct fluorinated epoxy-resin/alumina composite,” *IEEE Trans. Dielectr. Electr. Insul.*, vol. 23, no. 5, pp. 3071–3077, 2016.
- [3] Q. Xie, T. Wang, H. Huang, K. Fu, Y. Xu, and T. Shao, “Surface morphology and flashover performance of epoxy resin in SF6 after discharge aging,” *IEEE Trans. Dielectr. Electr. Insul.*, vol. 24, no. 6, pp. 3395–3404, 2017.

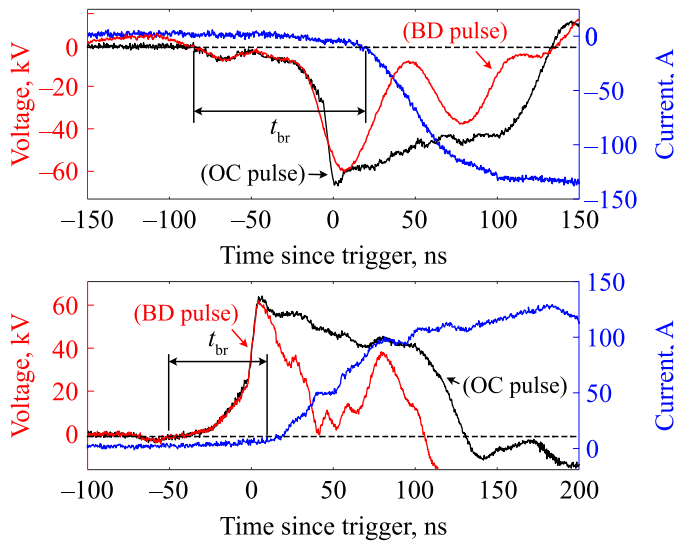


Fig. 10. Typical Open-circuit (OC) and Breakdown (BD) voltage waveforms for (top) negative, (bottom) positive voltage energisation using the Blumlein pulse generator. Blue curves (right axis) additionally show typical breakdown current waveforms for the Blumlein case. Indicated are points used to compute the time-to-breakdown,  $t_{br}$  as described in the main text.

[4] R. W. Macpherson, M. P. Wilson, I. V. Timoshkin, M. J. Given, and S. J. MacGregor, "Flashover of smooth and knurled dielectric surfaces in dry air," *IEEE Trans. Dielectr. Electr. Insul.*, vol. 31, no. 1, pp. 204–211, 2024.

[5] H. K. Meyer, R. Marskar, H. G. Osberg, and F. Mauseth, "Surface flashover over a microprofiled cylinder in air," *IEEE Trans. Dielectr. Electr. Insul.*, vol. 30, no. 6, pp. 2862–2869, 2023.

[6] J. Xue, H. Wang, J. Chen, K. Li, Y. Liu, B. Song *et al.*, "Effect of surface roughness on surface charge accumulation characteristics and surface flashover performance of alumina-filled epoxy resin spacers," *J. Appl. Phys.*, vol. 124, no. 8, p. 083302, 2018.

[7] Y. Zhao, Y. Xiang, S. Gu, B. Du, B. Dong, N. Xiang *et al.*, "Effect of surface roughness on flashover characteristics of silicone rubber," *J. Electrostat.*, vol. 99, pp. 41–48, 2019.

[8] Z. Zhan, Q. Zhang, F. Lü, Y. Liu, W. Liu, Z. Li *et al.*, "Effect of the surface roughness of epoxy resin on its creeping flashover characteristics in C4F7N-CO2 gas mixtures," *AIP Adv.*, vol. 9, no. 4, p. 045129, 2019.

[9] H. K. Meyer, F. Mauseth, R. Marskar, A. Pedersen, and A. Blaszczyk, "Streamer and surface charge dynamics in non-uniform air gaps with a dielectric barrier," *IEEE Trans. Dielectr. Electr. Insul.*, vol. 26, no. 4, pp. 1163–1171, 2019.

[10] H. K. Meyer, A. Blaszczyk, M. Schueller, F. Mauseth, and A. Pedersen, "Surface charging of dielectric barriers in short rod-plane air gaps—experiments and simulations," in *2018 IEEE Int. Conf. High Volt. Engr. Appl. (ICHVE)*, pp. 1–4, 2018.

[11] H. K. Meyer, F. Mauseth, A. Pedersen, and J. Ekeberg, "Breakdown mechanisms of rod-plane air gaps with a dielectric barrier subject to lightning impulse stress," *IEEE Trans. Dielectr. Electr. Insul.*, vol. 25, no. 3, pp. 1121–1127, 2018.

[12] R. Marskar and H. K. H. Meyer, "A kinetic monte carlo study of positive streamer interaction with complex dielectric surfaces," *Plasma Sources Sci. Technol.*, vol. 32, no. 8, p. 085010, 2023.

[13] J. O. Rossi, M. Ueda, A. R. Silva, and L. P. S. Neto, "Improvement on UHMWPE and PMMA Surface Flashover Under Atmospheric Pressure Using PIII Processing," *IEEE Trans. Plasma Sci.*, vol. 48, no. 10, pp. 3386–3391, Oct. 2020.

[14] H. K. H. Meyer, R. Marskar, and F. Mauseth, "Evolution of positive streamers in air over non-planar dielectrics: experiments and simulations," *Plasma Sources Sci. Technol.*, vol. 31, no. 11, p. 114006, 2022.

[15] J. M. Lehr, M. D. Abdalla, J. W. Burger *et al.*, "Design and development of a 1MV, compact, self break switch for high repetition rate operation," in *12th IEEE Int. Pulsed Power Conf.*, Monterey, CA, USA, Jun. 1999.

[16] "K-Modules: Modules designed for high energy X-ray or electron beam generating devices", Los Alamos National Laboratory. [Online]. Available: <https://www.lanl.gov/projects/feynman-center/technology->

[techsnapshots.php?id=61d66103f1b9050a1aab8ee9](https://www.lanl.gov/projects/feynman-center/technology-) (accessed Oct. 2024).

[17] R. A. H. Timmermans, H. C. Mastwijk, L. B. J. M. Berendsen, A. L. Nederhoff, A. M. Matser, M. A. J. S. Van Boekel *et al.*, "Moderate intensity Pulsed Electric Fields (PEF) as alternative mild preservation technology for fruit juice," *Int. J. Food Microbiol.*, vol. 298, pp. 63–73, Jun. 2019.

[18] "Square shoulder mills brochure: EMP02-040-A16-AP11-05C", ZCC Cutting Tools Europe GmbH. [Online]. Available: <https://www.zccct-europe.com> (accessed Oct. 2024).

[19] Drake Plastics Ltd. Co. (2019) Post curing torlon wear parts reduces wear. [Online]. Available: <https://drakeplastics.com/2019/03/25/> (accessed Oct. 2024).

[20] "Handysurf+: Portable, versatile surface texture measuring instrument", Accretech (Europe) GmbH. [Online]. Available: <https://www.accretech.eu/en/surface-measuring-systems/roughness-measuring-systems/handysurf-354045/> (accessed Oct. 2024).

[21] T. Wong, I. Timoshkin, S. MacGregor, M. Wilson, and M. Given, "The Breakdown and Surface Characteristics of Polymer Interfaces Under HV Impulses," *IEEE Trans. Dielectr. Electr. Insul.*, vol. 32, no. 1, pp. 170–179, Feb. 2025.

[22] I. C. Somerville, S. J. MacGregor, and O. Farish, "An efficient stacked-Blumlein HV pulse generator," *Meas. Sci. Technol.*, vol. 1, no. 9, pp. 865–868, Apr. 1990.

[23] *Geometric Product Specifications (GPS) - Surface texture: Profile method - Motif parameters ISO 12085, 1996.*

[24] J. A. Greenwood and J. B. P. Williamson, "Contact of nominally flat surfaces," *Proc. R. Soc. Lond. A Math. Phys. Sci.*, vol. 295, no. 1442, pp. 300–319, Dec. 1966.

[25] F. Robbe-Valloire, "Statistical analysis of asperities on a rough surface," *Wear*, vol. 249, no. 5–6, pp. 401–408, Jun. 2001.

[26] Quickfield Professional, version 6.4, Tera Analysis Ltd., [Online]. <https://quickfield.com/>

[27] S. Nijdam, J. Teunissen, and U. Ebert, "The physics of streamer discharge phenomena," *Plasma Sources Sci. Technol.*, vol. 29, no. 10, p. 103001, 2020.

[28] X. Li, A. Sun, G. Zhang, and J. Teunissen, "A computational study of positive streamers interacting with dielectrics," *Plasma Sources Sci. Technol.*, vol. 29, no. 6, p. 065004, 2020.

[29] A. Dubinova, "Modeling of streamer discharges near dielectrics," Ph.D. dissertation, Applied Physics and Science Education, Technische Universiteit Eindhoven, 2016, proefschrift.

[30] H. K. H. Meyer, R. Marskar, H. Gjemdal, and F. Mauseth, "Streamer propagation along a profiled dielectric surface," *Plasma Sources Sci. Technol.*, vol. 29, no. 11, p. 115015, 2020.



**Timothy Wong** (Member, IEEE) received the M.Eng degree in electrical and mechanical engineering with international study from the University of Strathclyde, Glasgow, U.K., in 2020, undertaking a one-year exchange with the Nanyang Technological University, Singapore. He subsequently received the degree of Ph.D. in electronic and electrical engineering from the UoS, where he remains based within the High Voltage Technologies Research Group as a Research Associate. His research interests include mathematical modelling of physical phenomena relevant to novel pulsed power and plasma technology, encompassing impulse-driven electrical breakdown, nonthermal plasma processes, and the optimisation of pulsed power systems. He is currently an associate member of the Institution of Mechanical Engineers (IMEchE), member of the IEEE Dielectrics and Electrical Insulation society (DEIS) and the IEEE Nuclear and Plasma Sciences society (NPSS). He is also a member of the IET. He was the recipient of multiple IEEE DEIS- and IEEE NPSS-sponsored conference awards including Best Poster, Best Presentation, and Outstanding Paper Awards conveyed at national and international conferences. In 2024, he received the NPSS Graduate Scholarship Award and was a recipient of an EPSRC Doctoral Prize Research Fellowship.



**Igor Timoshkin** (Senior Member, IEEE) received the degree in physics from Moscow State University, Moscow, Russia, in 1992, and the Ph.D. degree from the Imperial College of Science, Technology, and Medicine (ICSTM), London, U.K., in 2001. He was a researcher at Moscow State Agro Engineering University, Moscow, and then at the Institute for High Temperatures of Russian Academy of Sciences, Moscow. In 1997 he joined ICSTM. Then he joined the department of Electronic and Electrical Engineering, University of Strathclyde, Glasgow,

U.K., in 2001, where he became a Reader in 2016. His research interests include dielectric materials, pulsed power, transient spark discharges, environmental applications of non-thermal plasma discharges. Dr. Timoshkin was a Voting Member of the Pulsed Power Science and Technology Committee in the IEEE Nuclear and Plasma Science Society (2017-2021); currently he is a member of International Advisory Committee of the IEEE Conference on Dielectric Liquids, a member of the International Scientific Committee of the Gas Discharges and Their Applications Conference, and a Subject Editor of IET Nanodielectrics.



**Martin Given** (Senior Member, IEEE) received the B.Sc. degree in physics from the University of Sussex, Brighton, U.K., in 1981, and the Ph.D. degree in electronic and electrical engineering from the University of Strathclyde, Glasgow, U.K., in 1996. He is currently a Senior Lecturer with the Department of Electronic and Electrical Engineering, University of Strathclyde. His current research interests include ageing processes and condition monitoring in solid and liquid insulation systems, highspeed switching, and pulsed power.



**Scott MacGregor** (Senior Member, IEEE) received the B.Sc. and Ph.D. degrees from the University of Strathclyde, Glasgow, U.K., in 1982 and 1986, respectively. He was a Pulsed-Power Research Fellow in 1986 and a Lecturer in pulsed-power technology in 1989. In 1994, he became a Senior Lecturer, with a promotion to Reader and a Professor of High Voltage Engineering, in 1999 and 2001, respectively. In 2006 and 2010, he became the Head of the Department of Electronic and Electrical Engineering and the Executive Dean of the Faculty of Engineering,

and has been the Vice-Principal with the University of Strathclyde, since 2014. His current research interests include high-voltage pulse generation, high-frequency diagnostics, high power repetitive switching, high-speed switching, electronic methods for food pasteurization and sterilization, the generation of high-power ultrasound (HPU), plasma channel drilling, pulsed-plasma cleaning of pipes, and the stimulation of oil wells with HPU. Prof. MacGregor was a recipient of the 2013 IEEE Peter Haas Award. He was an Associated Editor of the IEEE Transactions of Dielectrics and Electrical Insulation in 2015.